Controlling the construction of trinuclear, 1-D, and 2-D Ni(II)Fe(II)/Fe(II)Fe(II) complexes: selective syntheses, structures, and magnetic properties

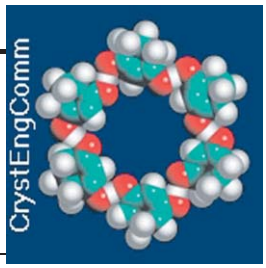

Paper

Asako Kamiyama, Tomoko Noguchi, Takashi Kajiwara* and Tasuku Ito*

Department of Chemistry, Graduate School of Science, Tohoku University, Aoba, Aramaki, Aoba-ku, Sendai 980-8578, Japan. E-mail: kajiwara@agnus.chem.tohoku.ac.jp

Received 3rd March 2003, Accepted 9th June 2003
First published as an Advance Article on the web 16th June 2003

The reaction of $[Ni(bpca)_2]$ (**1**) and $[Fe(H_2O)_6](ClO_4)_2$ gave a trinuclear complex **3**, five 1-D chain complexes **4a–e**, and a 2-D honeycomb complex **5**. The selective syntheses of these complexes were achieved by controlling the reaction conditions such as reaction stoichiometry, solvents, and the presence/absence of supporting ligands. **3** consists of a central $\{Fe(trans\text{-}H_2O)_2\}^{2+}$ moiety and two units of **1** acting as terminal bidentate ligands. **4a–e** consist of an alternating arrangement of Fe(II) ions and **1** which acts as a bis-bidentate bridging ligand. **5** has a honeycomb structure with hexagons involving twelve metal ions, six Ni(II) ions in **1** and six Fe(II) ions, and holds the large cavity which includes counter ions, chloroform, and water molecules. The reaction of $[Fe(bpca)_2]$ (**2**) and $[Fe(H_2O)_6](ClO_4)_2$ also gave a 2-D honeycomb complex **6** which is isostructural to **5**. Magnetic data for **3** and **4a** indicate a ferromagnetic interaction between adjoining Ni(II) ions and the Fe(II) ions, due to the strict orthogonality of the magnetic orbitals.

Introduction

Crystal engineering to form coordination networks and supramolecular architectures has been employed extensively to develop such abilities as catalysis,[1] magnetism,[2] electrical conductivity,[3] and gas adsorption.[4] As more potential applications are realized from assemblages of metal ions, the difficulty in controlling the structure of the assemblage becomes apparent. Complexed ligands can aid in the design and synthesis of metal complex assemblages and many examples have been reported.[5–8] Besides the construction of the various architectures, such as 1-D, 2-D, and 3-D complexes, it is also possible to tune the physical properties of an assemblage through a rational synthetic approach.

The organic ligand $bpca^-$ (Hbpca = bis(2-pyridylcarbonyl)-amine) is capable of being a bridging ligand *via* N_3 and O_2 sites which have different coordination abilities. The first reported polynuclear complex involving $bpca^-$ was a 1-D Cu(II) chain,[9] but, we recently showed that $[M(bpca)_2]$ (M = Mn(II), Fe(II), Ni(II), and Cu(II)) and $[M'(bpca)_2]^+$ (M′ = Cr(III), Fe(III), and Co(III)) can act as a building block to make polynuclear complexes in which different metal ions, or a metal ion in different environments, are arranged in an alternating manner.[10–14] $[M(bpca)_2]$ and $[M'(bpca)_2]^+$ can act as bis-bidentate ligands *via* four carbonyl sites, and their rigidity makes the design and construction of various structures easy. In this paper, we report the controlled syntheses and structures of a variety of multi-nuclear complexes using Fe(II) ion and $[M(bpca)_2]$ (M = Ni(II) (**1**) and M = Fe(II) (**2**)) in an alternate arrangement (Scheme 1). Using **1** as a complexed ligand, a discrete trinuclear complex **3**, five 1-D chain complexes **4a–e**, and a 2-D honeycomb complex **5**, which was communicated in part earlier,[12] were obtained, whereas a 2-D honeycomb complex **6** was obtained using a complexed ligand **2**. The magnetic properties of some of these complexes are also reported.

Experimental

All chemicals were reagent grade and used as received. **1**, **2**, **3** and **5** were synthesized according to the literature method.[12,13,15]

Preparation of *catena*-$[Fe^{II}\{Ni(bpca)_2\}(trans\text{-}MeOH)_2](ClO_4)_2\cdot 0.5dioxane\cdot 2MeOH$ (4a·0.5dioxane·2MeOH). To a solution of **1** (10 mg, 0.02 mmol) in $CHCl_3$/MeOH (1/1 (v/v), 2 cm^3) was added $[Fe(H_2O)_6](ClO_4)_2$ (7 mg, 0.02 mmol) in MeOH (0.4 cm^3). 1,4-dioxane was then allowed to diffuse slowly *via* vapor diffusion into the dark purple solution resulting in dark purple crystals of **4a**, which were collected and dried in the air (10 mg). IR (cm^{-1}): 1639 (C=O), 1091 (ClO_4^-).

Preparation of *catena*-$[Fe^{II}\{Ni(bpca)_2\}(cis\text{-}EtOH)_2](ClO_4)_2\cdot 3MeOH$ (4b·3MeOH). To a solution of **1** (10 mg, 0.02 mmol)

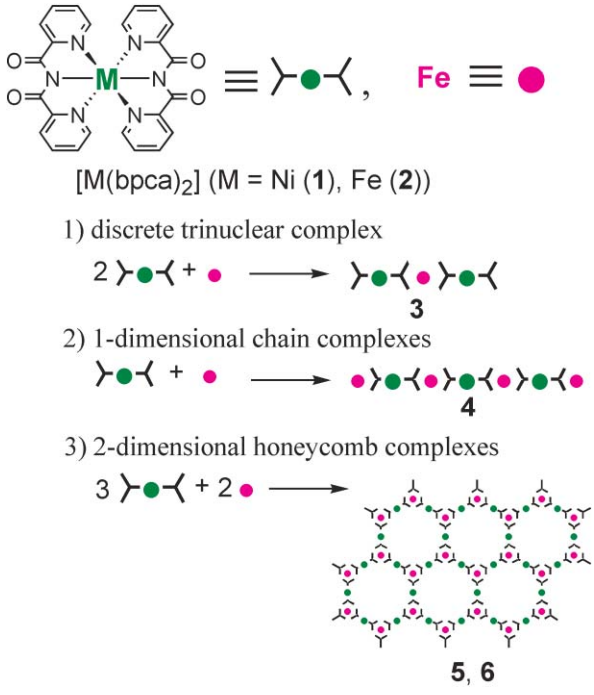

Scheme 1 Various structures constructed with $[M(bpca)_2]$.

DOI: 10.1039/b302413j

in $CHCl_3$ (1 cm^3) was added $[Fe(H_2O)_6](ClO_4)_2$ (7 mg, 0.02 mmol) in MeOH (1 cm^3) followed by one drop of EtOH. Dark purple crystals of **4b** were obtained by slow evaporation at room temperature, collected and dried in the air (10 mg). IR (cm^{-1}): 1639 (C=O), 1095 (ClO_4^-).

Preparation of *catena*-[Fe^{II}{Ni(bpca)$_2$}(HOC$_3$H$_6$OH-κ^2*O*)]-(ClO$_4$)$_2$·2MeOH·MeNO$_2$ (4c·2MeOH·MeNO$_2$). To a solution of **1** (10 mg, 0.02 mmol) in $CHCl_3$/$MeNO_2$ (1/1 (v/v), 2 cm^3) was added $[Fe(H_2O)_6](ClO_4)_2$ (7 mg, 0.02 mmol) in MeOH (0.8 cm^3). A few drops of 1,3-propanediol was added to the resulting dark purple solution. Black crystals of **4c** were obtained by slow evaporation at room temperature, collected and dried in the air (10 mg). IR (cm^{-1}): 1637 (C=O), 1091 (ClO_4^-).

Preparation of *catena*-[Fe^{II}(*trans*-NCS)$_2${Ni(bpca)$_2$}]·CHCl$_3$ (4d·CHCl$_3$). To a solution of **1** (10 mg, 0.02 mmol) in $CHCl_3$/MeOH (1/1 (v/v), 2 cm^3) was added $[Fe(H_2O)_6](ClO_4)_2$ (7 mg, 0.02 mmol) in MeOH (1 cm^3). A solution of NH_4NCS (8 mg, 0.1 mmol) in MeOH (0.5 cm^3) was added to the resulting dark purple solution. Black crystals of **4d** were obtained by slow evaporation at room temperature, collected and dried in the air (11 mg). IR (cm^{-1}): 1639 (C=O), 2073 (NCS^-).

Preparation of *catena*-[Fe^{II}Br{Ni(bpca)$_2$}(H$_2$O)]ClO$_4$·MeOH·0.75H$_2$O (4e·MeOH·0.75H$_2$O). To a solution of **1** (10 mg, 0.02 mmol) in $CHCl_3$/$MeNO_2$ (1/1 (v/v), 2 cm^3) was added $[Fe(H_2O)_6](ClO_4)_2$ (7 mg, 0.02 mmol) in MeOH (1 cm^3). A solution of *n*-Bu_4NBr (64 mg, 0.2 mmol) in MeOH (0.5 cm^3) was added to the resulting dark purple solution. Black crystals of **4e** were obtained by slow evaporation at room temperature, collected and dried in the air (9 mg). IR (cm^{-1}): 1639 (C=O), 1090 (ClO_4^-).

Preparation of complex [Fe^{II}_2{Fe(bpca)$_2$}$_3$](ClO$_4$)$_4$·5CHCl$_3$·2MeOH·7H$_2$O (6·5CHCl$_3$·2MeOH·7H$_2$O). The synthesis of **6** was carried out under N_2. $CHCl_3$ was distilled before use. To a solution of **2** (10 mg, 0.02 mmol) in $CHCl_3$/MeOH (1/1 (v/v), 2 cm^3) was added $[Fe(H_2O)_6](ClO_4)_2$ (4 mg, 0.01 mmol) in MeOH (0.4 cm^3). Black hexagonal crystals of **6** were obtained as a minor product by slow evaporation. Concomitantly, orange crystals and a white precipitate were also obtained, and the former was characterized as $[Fe(bpca)_2]ClO_4$, whereas the latter could not be characterized.

Crystal structure analyses

X-ray data for all complexes were collected at low temperature (180 to 220 K) with a Bruker AXS SMART-1000/CCD area detector using graphite monochromated Mo Kα radiation. The intensity data were empirically corrected for absorption by using the program SADABS.[16] The structures were solved by direct methods using SHELXS-86,[17] SIR92,[18] or by the Patterson method using DIRDIF94 (PATTY),[19] and the structure refinement was carried out using full-matrix least-squares (SHELXL-97[20]). Non-hydrogen atoms except for some solvent molecules were refined anisotropically while the hydrogen atoms were treated using a riding model. Final crystallographic data and the R_1 and wR_2 values are listed in Table 1.

CCDC reference numbers 205326–205331, 208260, 208261.

See http://www.rsc.org/suppdata/ce/b3/b302413j/ for crystallographic data in CIF or other electronic format.

Instrumentation

Fourier transform infrared spectroscopy was performed using a JASCO FT/IR-620 instrument as KBr pellets. Variable-temperature magnetic susceptibility measurements were made using a SQUID magnetometer MPMS 5S (Quantum Design) in a 1 T field for **4a**, and 0.5 T field for **3** and **5**. Diamagnetic correction for each sample was determined using Pascal's constants.

Results and discussion

Syntheses

The trinuclear complex **3**, the 1-D chain complexes **4a–e**, and the 2-D honeycomb complex **5** were obtained from the same starting materials, $[Ni(bpca)_2]$ (**1**) and $[Fe(H_2O)_6](ClO_4)_2$. The selective syntheses of these complexes were achieved by controlling the reaction conditions, such as stoichiometry, solvents, and so on, and these are summarized in Table 2.

Table 1 Crystallographic data for **3**, **4a–e**, **5**, and **6**

	3c	4a	4b	4c	4d	4e	5	6
Formula	$FeNi_2C_{48}H_{43}N_{12}O_{20.5}Cl_2$	$FeNiC_{29}H_{32}N_6O_{16.5}Cl_2$	$FeNiC_{31}H_{40}N_6O_{17}Cl_2$	$FeNiC_{30}H_{35}N_7O_{18}Cl_2$	$FeNiC_{27}H_{17}N_8O_4Cl_3S_2$	$FeNiC_{25}H_{23.5}N_6O_{10.75}ClBr$	$Fe_2Ni_3C_{78.5}H_{80.5}N_{18}O_{39}Cl_{17.5}$	$Fe_5C_{79}H_{75}N_{18}O_{37}Cl_{19}$
Fw	1360.11	914.07	954.15	967.11	802.52	809.92	2808.31	2821.37
Crystal system	Triclinic	Monoclinic	Monoclinic	Monoclinic	Monoclinic	Tetragonal	Orthorhombic	Orthorhombic
Space group	$P\bar{1}$	$P2_1/n$	$C2/c$	$C2/c$	$P2_1/c$	$I\bar{4}$	$Pnnm$	$Pnnm$
a/Å	8.9267(6)	10.1635(16)	10.4651(5)	10.4799(4)	9.7081(13)	14.9691(6)	32.999(2)	32.323(3)
b/Å	12.2683(8)	19.999(3)	18.6142(10)	19.5611(6)	19.095(3)		17.1473(11)	17.0606(14)
c/Å	13.3292(9)	20.833(3)	20.3093(11)	20.0708(7)	18.094(2)	30.3224(17)	20.9802(13)	20.7616(17)
α/°	90.215(2)							
β/°	101.813(2)	103.159(3)	102.8680(10)	103.6690(10)	98.035(3)			
γ/°	97.288(2)							
V/Å^3	1416.63(16)	4123.3(11)	3856.9(3)	3997.9(2)	3321.3(8)	6794.5(5)	11871.4(13)	11449.1(16)
Z	1	4	4	4	4	8	4	4
T/K	200	220	180	200	200	200	200	200
μ/mm^{-1}	1.092	1.011	1.086	1.051	1.417	2.297	1.184	1.147
R_1[a] ($>2\sigma(I)$)	0.0616	0.0733	0.0440	0.0396	0.0675	0.0675	0.0854	0.0787
wR_2[b] ($>2\sigma(I)$)	0.1428	0.1789	0.1230	0.1040	0.1897	0.1563	0.2488	0.2145
R_1[a] (all data)	0.1241	0.2003	0.0640	0.0581	0.1197	0.1320	0.1578	0.1567
wR_2[b] (all data)	0.1688	0.2366	0.1343	0.1123	0.2175	0.1825	0.2994	0.2617

[a] $R_1 = \Sigma \||F_o| - |F_c|\|/\Sigma |F_o|$. [b] $wR_2 = [\Sigma w (F_o^2 - F_c^2)^2/\Sigma w (F_o^2)^2]^{1/2}$.

Table 2 Experimental conditions

		1/Fe(II)	Solvents	Additional ligand
3	$[Fe(\mathbf{1})_2(trans\text{-}H_2O)_2](ClO_4)_2$	2/1	$CHCl_3$/MeOH	Water
4a[a]	*catena*-$[Fe(\mathbf{1})(trans\text{-}MeOH)_2](ClO_4)_2$	1/1	$CHCl_3$/MeOH	
4b	*catena*-$[Fe(\mathbf{1})(cis\text{-}EtOH)_2](ClO_4)_2$	1/1	$CHCl_3$/MeOH	EtOH
4c	*catena*-$[Fe(\mathbf{1})(HOC_3H_6OH\text{-}\kappa^2O)](ClO_4)_2$	1/1	$CHCl_3/MeNO_2$/MeOH	1,3-propanediol
4d	*catena*-$[Fe(trans\text{-}NCS)_2(\mathbf{1})]$	1/1	$CHCl_3/MeNO_2$/MeOH	NH_4NCS
4e	*catena*-$[FeBr(\mathbf{1})(H_2O)]ClO_4$	1/1	$CHCl_3/MeNO_2$/MeOH	*n*-Bu_4NBr
5	$[Fe_2(\mathbf{1})_3](ClO_4)_4$	2/1	Distilled $CHCl_3$/MeOH	

[a] **4a** was obtained by the diffusion of 1,4-dioxane.

When **1** and Fe(II) were reacted in a $CHCl_3$/EtOH solution, a dark purple precipitate immediately formed, which is independent of the reaction stoichiometry. The reaction between **1** and $[Fe(EtOH)_6]^{2+}$ forms insoluble polymers. However, in a mixture of $CHCl_3$/MeOH, adducts of **1** and $[Fe(MeOH)_6]^{2+}$ are very soluble and syntheses of **3**–**5** were possible.

Controlling the reaction conditions led to the formation of **3** (**1**/Fe(II) = 2/1) and **4a–e** (1/1). The presence/absence of supporting ligands such as alcohol and (pseudo)halide ion also affects the formation of products. As two water molecules are coordinated to the Fe(II) ion in **3** (*vide infra*), the synthesis must be carried out with an excess of water. **4a–e** were obtained by the reaction of **1**/Fe(II) in 1/1 reaction ratio in $CHCl_3$/MeOH or $CHCl_3$/MeOH/$MeNO_2$. When 1,4-dioxane was added *via* vapor diffusion, **4a** was precipitated. **4b–e** were prepared by adding an excess amount of EtOH, HOC_3H_6OH, NCS^-, or Br^-, respectively.

When the molar ratio of **1**/Fe(II) was 3/2, which is equal to the composition of **5**, a mixture of **4b** and **5** resulted. Because the trinuclear unit $\{Fe(\mathbf{1})_2\}^{2+}$ is stable in solution and a significant amount of free Fe(II) ions is present in this reaction,[12] **4b** can quite easily form through successive reactions of the two species. To avoid the formation of **4b**, the ratio of **1**/Fe(II) must be 2 or larger. Moreover since a small amount of EtOH acts as a supporting ligand in **4b**, $CHCl_3$ should be distilled beforehand to remove EtOH used as a stabilizer.

6 was synthesized in a similar manner to **5** by replacing $[Ni(bpca)_2]$ (**1**) with $[Fe(bpca)_2]$ (**2**). To avoid the oxidation of **2**, the reaction was carried out under N_2. However, orange crystals and white precipitates were also isolated from this reaction, and **6** was only a minor product. The orange crystals were identified as $[Fe(bpca)_2]ClO_4$ by their IR spectrum, but the white precipitates could not be characterized. The yield of **6** is low because **2** can be easily oxidized to $\mathbf{2}^+$.[14,15]

Structure of trinuclear complex, 3

The structure of **3**, Fig. 1, is comprised of two units of $\{Ni(bpca)_2\}$ (**1**) acting as terminal ligands and a central $\{Fe(H_2O)_2\}^{2+}$. Selected atom–atom distances are summarized in Table 3 along with selected bond distances for **1**. The cationic part of the asymmetric unit has one unit of **1**, one water molecule and the Fe(II) which lies on a crystallographic inversion center.

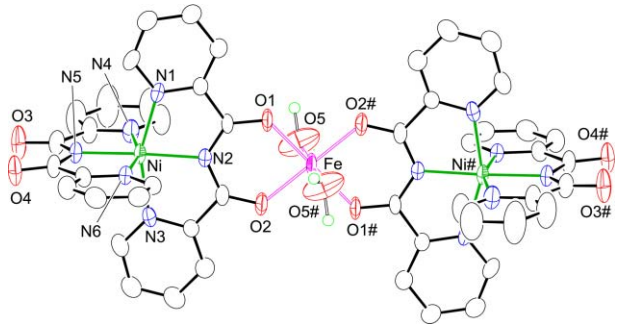

Fig. 1 ORTEP drawings of **3** with thermal ellipsoids at 50% probability. Hydrogen atoms are omitted for clarity. The moiety with solid bonds represents the $\{Ni(bpca)_2\}$ unit, whereas the other is the $\{Fe(trans\text{-}H_2O)_2\}^{2+}$ unit. Green, purple, blue, and red spheres represent Ni(II), Fe(II), N, and O, respectively. Symmetry codes: (#) $-x$, $-y$, $-z$. Click here to access a 3D representation.

Table 3 Selected atom–atom distances (Å) in **1** and **3**

	Bound C=O site in **3**	Unbound C=O site in **3**	**1**[a]
$Ni–N_{amide}$	2.034(3)	2.007(3)	2.0246(17)
$Ni–N_{py}$	2.122(4), 2.116(4)	2.079(4), 2.089(4)	2.1001(15)
C–O	1.252(5), 1.247(5)	1.235(5), 1.214(5)	1.224(2)
$C–N_{amide}$	1.348(6), 1.345(6)	1.351(6), 1.366(6)	1.364(2)
$Fe–O_{bpca^-}$	2.019(3), 2.065(3)		
$Fe–O_{water}$	2.107(6)		
Ni–Fe	5.3679(6)		

[a] Ref. 13.

In **3**, each **1** moiety has two sets of C=O groups where the oxygen atoms are bound (O1 and O2) to the Fe(II) center and unbound (O3 and O4). The C=O groups bound to the Fe(II) ion have slightly longer bond lengths (1.252(5) and 1.247(5) Å) than the unbound ones (1.235(5) and 1.214(5) Å). The Ni(II) ion is surrounded by four pyridyl nitrogens and two amide nitrogens, and the $Ni–N_{amide}$ bond distance near the bound C=O is longer than that near the unbound C=O ($Ni–N_{amide}$ = 2.034(3) Å for bound C=O site; 2.007(3) Å for unbound C=O site). When the C=O groups of a $bpca^-$ ligand coordinate to another metal ion, the negative charge of central N_{amide} delocalizes into the O–C–N–C–O conjugated system, and the change in electronic structure is observed as an elongation both in the C=O and the $Ni–N_{amide}$ bonds. The central Fe(II) ion is in an axially elongated octahedron surrounded by four equatorial O_{bpca^-} atoms and two axial O_{water} atoms ($Fe–O_{bpca^-}$ = 2.019(3), 2.065(3) Å and $Fe–O_{water}$ = 2.107(6) Å, respectively).

Structures of 1-D complexes, 4a–e

Fig. 2 shows the structures of **4a–c**, and Fig. 3 shows **4d** and **4e**, respectively. The selected atom–atom distances are summarized in Tables 4 and 5. The 1-D chain complexes **4a–c** consist of $\{Ni(bpca)_2\}$ (**1**) and $\{Fe(alcohol)_n\}^{2+}$ moieties in an alternating arrangement. **1** acts as a bis-bidentate bridging complexed ligand *via* the two sets of two carbonyl groups. **4a–c** are discriminated by the different alcohol ligands (two MeOH (**4a**), two EtOH (**4b**), and a 1,3-propanediol (**4c**)) with the different coordination geometry (*trans* in **4a**, *cis* in **4b** and **4c**). **4d** and **4e** also have alternating chain structures with $\{Ni(bpca)_2\}$ (**1**) and $\{Fe(trans\text{-}NCS)_2\}$ for **4d** and $\{FeBr(H_2O)\}^+$ for **4e**, respectively. Upon forming the chain complexes, the C–O distances in **4a–e** are elongated by *ca.* 0.02 Å compared with those in **1** which results from the delocalization of the negative charge on the O–C–N–C–O moiety (*vide supra*). However, the distances around the Ni(II) ion in **4a–e**, $Ni–N_{amide}$ and $Ni–N_{py}$, are essentially not influenced upon the coordination.

4a consists of **1** and $\{Fe(trans\text{-}MeOH)_2\}^{2+}$ moiety. The Fe(II) coordination geometry is slightly elongated octahedral with four oxygen atoms from two $bpca^-$ ligands in the equatorial

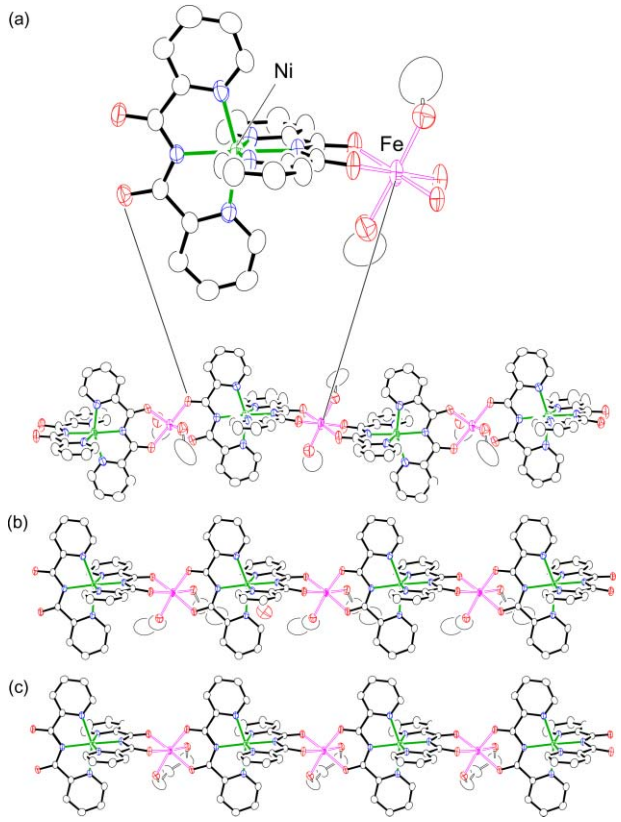

Fig. 2 ORTEP drawings of cationic parts of (a) **4a**, (b) **4b**, and (c) **4c** with thermal ellipsoids at 50% probability. Hydrogen atoms are omitted for clarity. The moieties with solid bonds represent the $\{Ni(bpca)_2\}$ units, whereas others are {Fe} units. Green, purple, blue, and red spheres represent Ni(II), Fe(II), N, and O, respectively. Click here to access a 3D representation of **4b**.

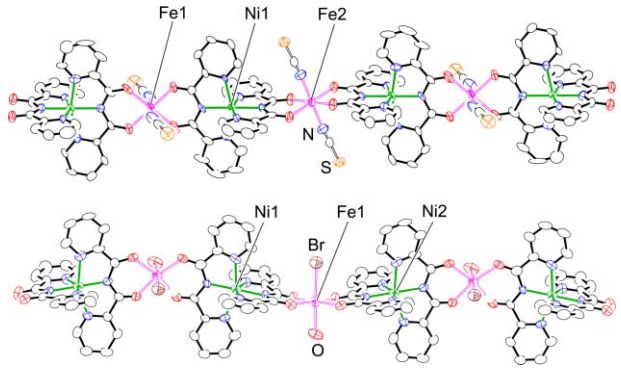

Fig. 3 ORTEP drawings of cationic parts of (top) **4d** and (bottom) **4e** with thermal ellipsoids at 50% probability. Hydrogen atoms are omitted for clarity. The moieties with solid bonds represent the $\{Ni(bpca)_2\}$ units, whereas others are {Fe} units. Green, purple, blue, red, orange, and brown spheres represent Ni(II), Fe(II), N, O, S, and Br, respectively. Click here to access a 3D representation of **4d**.

Table 5 Selected atom–atom distances (Å) in **4d** and **4e**

	4d	**4e**
$Ni–N_{amide}$	2.010(4), 2.008(4)	2.019(8), 2.018(8)
$Ni–N_{py}$	2.094(4)–2.112(4)	2.097(9)–2.132(9)
C–O	1.223(6)–1.247(6)	1.211(12)–1.242(12)
$C–N_{amide}$	1.348(6)–1.362(6)	1.338(14)–1.375(13)
$Fe–O_{bpca–}$	2.071(4)–2.082(4)	2.051(7)–2.069(7)
$Fe–O_{water}$		2.212(8)
Fe–Br		2.611(2)
$Fe–N_{NCS–}$	2.110(5), 2.100(5)	
Ni–Fe	5.3376(8), 5.3794(8)	5.3707(16), 5.3696(16)

plane with the distances of 2.0510(18)–2.0642(18) Å, and two oxygen atoms from the coordinating MeOH molecules in the axial positions with the distances of 2.140(2) and 2.134(2) Å.

4b and **4c** are crystallographically isostructural to each other possessing an $\{Fe(\mathbf{1})(cis\text{-}EtOH)_2\}^{2+}$ moiety in **4b** and an $\{Fe(\mathbf{1})(HOC_3H_6OH\text{-}\kappa^2O)\}^{2+}$ moiety in **4c**, respectively. The cationic part of the asymmetric unit in **4b** and **4c** consists of half of these moieties, and there are crystallographic 2-fold axes residing on the Ni(II) and Fe(II) atoms. The Fe(II) has a distorted octahedral coordination geometry with four oxygen atoms from two $bpca^-$ ligands and two oxygen atoms from the coordinating alcohol molecules. Two EtOH molecules are *cis* to each other in **4b**, and HOC_3H_6OH forms a six membered chelate ring in **4c**. The Fe(II) atoms in **4b** and **4c** deviate slightly from the mean plane of $bpca^-$ ligand (0.49(1) Å for **4b** and 0.51(1) Å for **4c**, respectively). In both complexes, the $Fe–O_{bpca–}$ distances are shorter than the $Fe–O_{alcohol}$ distances by *ca.* 0.05 Å.

4d consists of **1** and $\{Fe(trans\text{-}NCS)_2\}$ moiety in an alternating arrangement. The asymmetric unit contains three metal centers, Fe1–Ni1–Fe2, and both Fe(II) ions lie on a crystallographic inversion center. Fe(II) is in an axially elongated octahedron with four oxygen atoms from two $bpca^-$ ligands in an equatorial plane (2.071(4)–2.082(4) Å) and two nitrogen atoms from NCS^- ligands in axial positions (2.110(5)–2.100(5) Å).

4e consists of **1** and $\{FeBr(H_2O)\}^+$ moiety. The cationic part of the asymmetric unit contains three metal centers, Ni1–Fe1–Ni2, and both Ni(II) ions lie on a crystallographic 2-fold axes. Fe(II) is surrounded by four oxygen atoms from two $bpca^-$ ligands in an equatorial plane (2.051(7)–2.069(7) Å), and one oxygen atom from the coordinating H_2O molecule (2.212(8) Å) and a Br^- (2.611(2) Å) in axial positions. The $Fe–O_{water}$ distance is longer than the $Fe–O_{bpca–}$ distances by *ca.* 0.15 Å. The Fe–Br distance in **4e** is longer than the usual Fe–Br bond (2.30–2.40 Å), and hence the coordination of Br^- in this complex is weak. Thus the coordination geometry around Fe(II) is axially elongated octahedral.

Structures of 2-D complexes, 5 and 6

Since the structure of **5** was reported previously,[12] we describe here in detail with **6**. Fig. 4 shows the structure of **6**, and selected atom–atom distances for **5** and **6** are summarized in Table 6. **5** and **6** are crystallographically isostructural to each

Table 4 Selected atom–atom distances (Å) in **4a**, **4b**, and **4c**

	4a	**4b**	**4c**
$Ni–N_{amide}$	2.0109(16), 2.0080(16)	2.027(2)	2.0176(11)
$Ni–N_{py}$	2.094(2)–2.110(2)	2.110(3), 2.099(2)	2.1029(10), 2.1028(11)
C–O	1.231(2)−1.242(3)	1.238(3), 1.242(3)	1.2444(15), 1.2445(16)
$C–N_{amide}$	1.343(3)−1.365(3)	1.348(4), 1.352(4)	1.3529(15), 1.3461(17)
$Fe–O_{bpca–}$	2.0510(18)−2.0642(18)	2.080(2), 2.083(2)	2.0798(10), 2.0754(8)
$Fe–O_{alcohol}$	2.140(2), 2.134(2)	2.141(2)	2.1287(10)
Ni–Fe	5.3126(8)	5.3339(3)	5.3247(2)

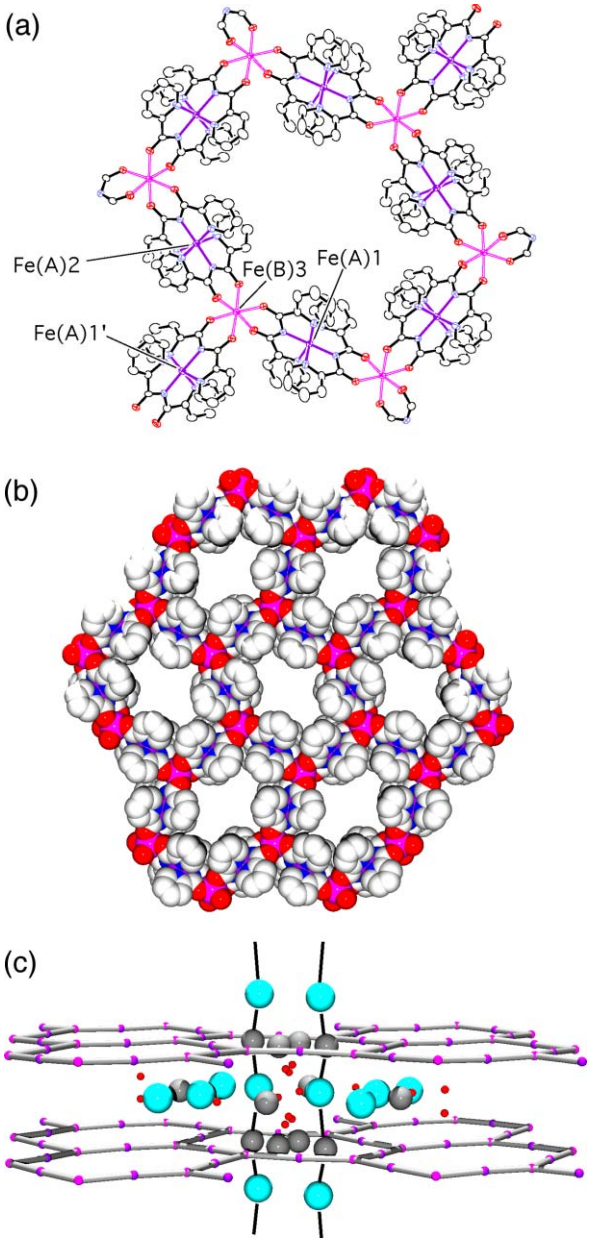

Fig. 4 (a) ORTEP drawing with thermal ellipsoids at 50% probability and (b) space filling drawing of **6**. Hydrogen atoms are omitted. (c) Schematic drawing of counter anions and crystal solvents in **6**. Blue, gray, and red spheres represent ClO_4^-, $CHCl_3$, and H_2O, respectively. Symmetry codes: (′) $-x+1/2$, $y-1/2$, $-z+1/2$. Click here to access a 3D representation of **6**.

Table 6 Selected atom–atom distances (Å) in **5** and **6**

	5 (M = Ni)	**6** (M = Fe)
M–N_{amide}	2.0121(15)–2.0196(15)	1.9279(16)–1.9403(16)
M–N_{py}	2.0810(17)–2.1142(16)	1.9557(17)–1.9778(17)
C–O	1.240(2)–1.247(2)	1.230(2)–1.255(2)
C–N_{amide}	1.332(2)–1.362(2)	1.341(3)–1.365(3)
Fe–O_{bpca^-}	2.0614(14)–2.1081(13)	2.0561(15)–2.1052(14)
M–Fe	5.4238(4), 5.3863(4)	5.3210(5), 5.2855(5)

other. Both complexes contain $(6,3)$[21] nets with the composition of $[Fe_2\{Ni(bpca)_2\}_3]^{4+}$ for **5** and $[Fe_2\{Fe(bpca)_2\}_3]^{4+}$ for **6**, respectively, which spread out over the *ab* plane. The honeycomb layer consists of edge-sharing hexagons with a triply chelated Fe(II) ion at each corner and a bridging complexed ligand at each edge coordinating in a bis-bidentate fashion. In **5**, the ring structure contains twelve metal ions, six Ni(II) ions from $[Ni(bpca)_2]$ (**1**) and six Fe(II) ions to form a large cavity with the largest diagonal separations of Ni–Ni = 21.5834(11) Å and Fe–Fe = 16.4629(9) Å. The cavity size was estimated from a space filling model to be *ca.* 12 Å along the Ni–Ni axis and *ca.* 13 Å along the Fe–Fe axis. **6** also has a ring structure with twelve Fe(II) ions, and the largest diagonal separations are 20.8349(14) and 16.6331(12) Å, respectively. **5** and **6** show non-interpenetrating networks regardless of the presence of the large cavities owing to the steric repulsion of pyridyl groups in the $bpca^-$ ligands.

In **5**, Ni(II) ion is in a distorted octahedron with six nitrogen atoms, four pyridyl nitrogens and two amide nitrogens, and the distances around the Ni(II) ion are almost similar to those in **1**. Fe(II) ion is bonded to six oxygen atoms arising from three $bpca^-$, and the average distance of the Fe–O bonds is 2.08 Å. **6** contains two kinds of Fe(II) ions, Fe(A) in the complexed ligand $[Fe(bpca)_2]$ (**2**) surrounded by six nitrogen atoms and Fe(B) surrounded by six oxygen atoms. The average coordination distance of Fe(A) is 1.95 Å, which is typical for the low spin Fe(II) ion similar to those in **2**.[13] On the other hand, the average value of the Fe–O distances for Fe(B) is 2.08 Å being consistent with a high spin Fe(II) ion. The elongation of C=O distances in **5** and **6** compared with **1** and **2**, respectively, were also observed (*vide infra*).

The layers are superimposed along the *c* axis. Neighboring layers are related by a crystallographic mirror plane perpendicular to the *c* axis, and **5** and **6** show a complete channel structure along the *c* axis. ClO_4^- ions, $CHCl_3$, MeOH, and H_2O molecules are present between the layers. A half of ClO_4^- forms a 1-D chain structure with $CHCl_3$ molecules, which penetrate the channel (Fig. 4c).

The Fe(II) ion sits on an O_6 octahedron with a chiral environment (Δ or Λ), and a single layer consists of only one of the two optical isomers. Neighboring layers have the opposite chirality, *i.e.*, the chirality of all Fe(II) ions in the first layer is Δ and in the next, Λ.

Magnetic properties

The temperature dependent magnetic susceptibilities of **3**, **4a**, and **5**, which contain $\{Ni(bpca)_2\}$ (**1**) and Fe(II), were measured down to 2 K. Fig. 5a shows the magnetic data for **3**. The $\chi_m T$ is nearly constant in the temperature range from 300 to 80 K with a value of *ca.* 6.0 cm^3 K mol^{-1}, which is related to the dilute three magnetic centers ($S = 1$ for Ni(II) and 2 for high spin Fe(II)) with an average g value of 2.19. On lowering the temperature, the $\chi_m T$ values gradually increase below 80 K, reaching 6.84 cm^3 K mol^{-1} at 14 K, and then decrease rapidly. The swift decrease of $\chi_m T$ values at low temperature is mainly due to the zero-field splitting of Fe(II) ion as well as two terminal Ni(II) ions. The magnetic behavior for **3** suggests a ferromagnetic interaction between adjoining Ni(II) and Fe(II) ions through the chelating O–C–N–C–O moiety. The magnetic data of **3** were analyzed by the three-spin model with an exchange coupling constant J ($H = -2J(S_{Ni1}S_{Fe2}+S_{Fe2}S_{Ni3})$)[22] above 20 K to avoid influence from zero-field splitting. The least squares calculation yielded best fit parameters of $g = 2.19(1)$ and $J = +0.56(1)$ cm^{-1}.

Fig. 5b shows the magnetic data for **4a**. The $\chi_m T$ value of *ca.* 4.9 cm^3 K mol^{-1} at room temperature is slightly larger than the spin only value of 4.00 cm^3 K mol^{-1} for a Ni(II) ion and a high spin Fe(II) ion with a g value of 2.0. On lowering the temperature, the $\chi_m T$ values remain constant, gradually increase below 75 K, reaching 5.47 cm^3 K mol^{-1} at 15 K, and then decrease rapidly. The swift decrease of $\chi_m T$ values at low temperature is again due to zero-field splitting of the Fe(II) and Ni(II) ions. The ferromagnetic behavior of **4a** was analyzed by the Curie–Weiss model with the data between 20 to 250 K, and the least squares calculation yielded best fit parameter of $\theta = +1.6(3)$ K.

The $\chi_m T$ value of **5** is almost constant in the range of 40 to

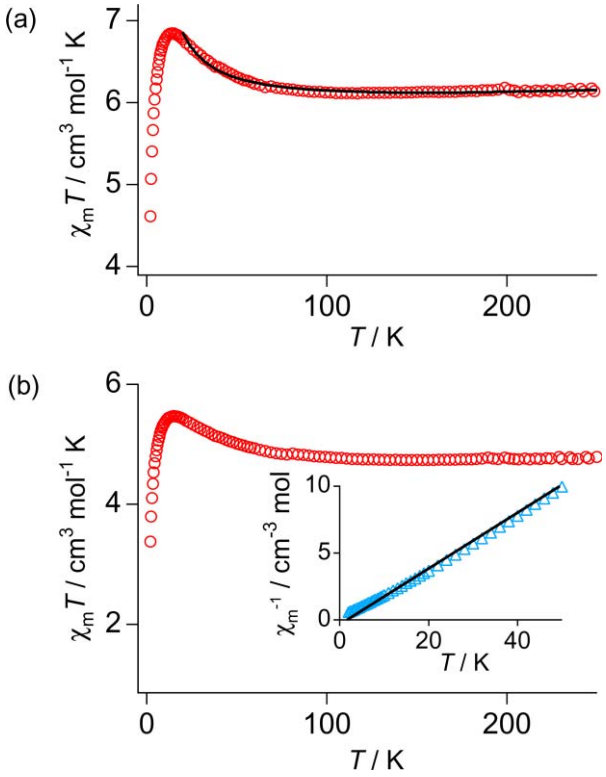

Fig. 5 (a) A plot of $\chi_m T$ *vs.* T for **3**. Solid line corresponds to the theoretical curve for which parameters are given in the text. (b) A plot of $\chi_m T$ *vs.* T and a plot of χ_m^{-1} *vs.* T (inset) for **4a**. Solid line corresponds to the theoretical curve for which parameters are given in the text.

300 K with a value of *ca.* 9 cm^3 K mol^{-1}, similar to the spin only value. This result indicates that the magnetic interaction between Ni(II) and Fe(II) in **5** is very small and can be neglected. Below 40 K, the $\chi_m T$ value decreases rapidly caused by the zero-field splitting.

Ni(II) ion has two dσ spins in the e_g orbitals in the O_h formalism, while an Fe(II) ion has both dσ spins in e_g orbitals and dπ spins in t_{2g} orbitals. In these complexes, the Ni(II) and Fe(II) ions are bridged by bpca$^-$ ligand in a κ^3N:κ^2O bridging manner with local C_2 symmetry. The e_g (Ni) and e_g (Fe) orbitals have different symmetry about the 2-fold rotation involving the Ni–Fe axis, *i.e.* the former is symmetric, whereas the latter is antisymmetric. Hence, these two e_g orbitals are orthogonal to each other, which is advantageous for ferromagnetic coupling between Ni(II) and Fe(II) ions. On the other hand, e_g (Ni) and t_{2g} (Fe) are both symmetric and have a non-zero overlap integral, which leads to antiferromagnetic coupling. The net magnetic interaction arise from the sum of these two opposite interactions. In **3** and **4a**, the ferromagnetic interaction (e_g (Ni)–e_g (Fe)) slightly dominates over the antiferromagnetic interaction (e_g (Ni)–t_{2g} (Fe)), and a weak ferromagnetic interaction occurs as we have already reported.[13] **5** did not show any significant magnetic interactions, which is caused by an almost equal contribution of ferro- and antiferromagnetic interactions. These differences in magnetic interactions may be due to a subtle change in the coordination geometry around Fe(II).

Conclusion

It was possible to selectively synthesize a trinuclear complex **3**, 1-D complexes **4a–e**, and 2-D complexes **5** and **6**. Although the starting materials for the most of the complexes (**3**, **4a–e** and **5**) are the same, the selective syntheses were achieved by controlling the reaction conditions, such as the reaction stoichiometry and solvents. **6** was obtained similarly to **5** using complexed ligand **2** instead of **1**. The magnetic data for **3** and **4a** showed the presence of a ferromagnetic interaction between adjoining Ni(II) and Fe(II) ions through the bpca$^-$ ligand.

Acknowledgements

This work was supported by Grants-in-Aid for Scientific Research on Priority Areas (No. 10149102) and for Encouragement of Young Scientists (No. 13740370) from the Ministry of Education, Culture, Sports, Science, and Technology, Japan, as well as by JSPS Research Fellowships for Young Scientists (No. 12006281).

References

1 (*a*) A. S. Larsen, K. Wang, M. A. Lockwood, G. L. Rice, T.-J. Won, S. Lovell, M. Sadílek, F. Turecek and J. M. Mayer, *J. Am. Chem. Soc.*, 2002, **124**, 10112; (*b*) G. Süss-Fink, M. Faure and T. R. Ward, *Angew. Chem., Int. Ed.*, 2002, **41**, 99.
2 (*a*) J. L. Manson, Q.-z. Huang, J. W. Lynn, H.-J. Koo, M.-H. Whangbo, R. Bateman, T. Otsuka, N. Wada, D. N. Argyriou and J. S. Miller, *J. Am. Chem. Soc.*, 2001, **123**, 162; (*b*) A. Caneschi, D. Gatteschi, N. Lalioti, C. Sangregorio, R. Sessoli, G. Venturi, A. Vindigni, A. Rettori, M. G. Pini and M. A. Novak, *Angew. Chem., Int. Ed.*, 2001, **40**, 1760; (*c*) B. Moulton, J. Lu, R. Hajndl, S. Hariharan and M. J. Zaworotko, *Angew. Chem., Int. Ed.*, 2002, **41**, 2821; (*d*) O. Kahn, J. Larionova and J. V. Yakhmi, *Chem. Eur. J.*, 1999, **5**, 3443.
3 (*a*) H. Tanaka, Y. Okano, H. Kobayashi, W. Suzuki and A. Kobayashi, *Science*, 2001, **291**, 285; (*b*) M. Mitsumi, T. Murase, H. Kishida, T. Yoshinari, Y. Ozawa, K. Toriumi, T. Sonoyama, H. Kitagawa and T. Mitani, *J. Am. Chem. Soc.*, 2001, **123**, 11179.
4 (*a*) S. Noro, S. Kitagawa, M. Kondo and K. Seki, *Angew. Chem., Int. Ed.*, 2000, **39**, 2081; (*b*) H. Li, M. Eddaoudi, M. O'Keeffe and O. M. Yaghi, *Nature*, 1999, **402**, 276.
5 (*a*) M. Ohba, N. Usuki, N. Fukita and H. Ōkawa, *Angew. Chem., Int. Ed.*, 1999, **38**, 1795; (*b*) N. Shimamoto, S. Ohkoshi, O. Sato and K. Hashimoto, *Inorg. Chem.*, 2002, **41**, 678; (*c*) J. T. Culp, J.-H. Park, D. Stratakis, M. W. Meisel and D. R. Talham, *J. Am. Chem. Soc.*, 2002, **124**, 10083.
6 (*a*) T. Nakamoto, Y. Miyazaki, M. Itoi, Y. Ono, N. Kojima and M. Sorai, *Angew. Chem., Int. Ed.*, 2001, **40**, 4716; (*b*) S. Bénard, P. Yu, J. P. Audière, E. Rivière, R. Clèment, J. Guilhem, L. Tchertanov and K. Nakatani, *J. Am. Chem. Soc.*, 2000, **122**, 9444; (*c*) E. Coronado, J.-R. Galán-Mascarós, C.-J. Gómez-García, J. Ensling and P. Gütlich, *Chem. Eur. J.*, 2000, **6**, 552; (*d*) E. Coronado, J. R. Galán-Mascarós, C.-J. Gómez-García and J. M. Martínez-Agudo, *Inorg. Chem.*, 2001, **40**, 113; (*e*) H. Tamaki, Z. J. Zhong, N. Matsumoto, S. Kida, M. Koikawa, N. Achiwa, Y. Hashimoto and H. Ōkawa, *J. Am. Chem. Soc.*, 1992, **114**, 6974.
7 (*a*) H. O. Stumpf, L. Ouahab, Y. Pei, D. Grandjean and O. Kahn, *Science*, 1993, **261**, 447; (*b*) H. O. Stumpf, L. Ouahab, Y. Pei, P. Bergerat and O. Kahn, *J. Am. Chem. Soc.*, 1994, **116**, 3866; (*c*) M. G. F. Vaz, L. M. M. Pinheiro, H. O. Stumpf, A. F. C. Alcântara, S. Golhen, L. Ouahab, O. Cador, C. Mathonière and O. Kahn, *Chem. Eur. J.*, 1999, **5**, 1486.
8 (*a*) F. Birkelbach, U. Flörke, H.-J. Haupt, C. Butzlaff, A. X. Trautwein, K. Wieghardt and P. Chaudhuri, *Inorg. Chem.*, 1998, **37**, 2000; (*b*) D. Burdinski, F. Birkelbach, T. Weyhermüller, U. Flörke, H.-J. Haupt, M. Lengen, A. X. Trautwein, E. Bill, K. Wieghardt and P. Chaudhuri, *Inorg. Chem.*, 1998, **37**, 1009; (*c*) D. Burdinski, E. Bill, F. Birkelbach, K. Wieghardt and P. Chaudhuri, *Inorg. Chem.*, 2001, **40**, 1160.
9 A. Cantarero, J. M. Amigó, J. Faus, M. Julve and T. Debaerdemaeker, *J. Chem. Soc., Dalton Trans.*, 1988, 2033.
10 T. Kajiwara and T. Ito, *J. Chem. Soc., Dalton Trans.*, 1998, 3351.
11 T. Kajiwara and T. Ito, *Mol. Cryst. Liq. Cryst.*, 1999, **335**, 73.
12 A. Kamiyama, T. Noguchi, T. Kajiwara and T. Ito, *Angew. Chem., Int. Ed.*, 2000, **39**, 3130.
13 A. Kamiyama, T. Noguchi, T. Kajiwara and T. Ito, *Inorg. Chem.*, 2002, **42**, 507.
14 T. Kajiwara, R. Sensui, T. Noguchi, A. Kamiyama and T. Ito, *Inorg. Chim. Acta*, 2002, **337**, 299.
15 S. Wocadlo, W. Massa and J.-V. Jolgado, *Inorg. Chim. Acta*, 1993, **207**, 199.
16 G. M. Sheldrick, *SADABS, Program for Empirical Absorption Correction of Area Detector Data*, University of Göttingen, Germany, 1996.

17 G. M. Sheldrick, *SHELXS-86*, University of Göttingen, Göttingen, Germany, 1986.
18 A. Altomare, M. C. Burla, M. Camalli, M. Cascarano, C. Giacovazzo, A. Guagliardi and G. Polidori, *J. Appl. Crystallogr.*, 1994, **27**, 435.
19 P. T. Beurskens, G. Admiraal, W. P. Bosman, R. D. Gelder, R. Israel and J. M. M. Smits, *The DIRDIF-94 program system*, Technical Report of the Crystallography Laboratory, University of Nijmegen, the Netherlands, 1994.
20 G. M. Sheldrick, *SHELXL-97, Program for refinement of crystal structures*, University of Göttingen, Germany, 1997.
21 S. R. Batten and R. Robson, *Angew. Chem., Int. Ed.*, 1998, **37**, 1460.
22 O. Kahn, *Molecular Magnetism*, VCH Publishers, Weinheim, 1993.